Materials Horizons

ROYAL SOCIETY OF CHEMISTRY

COMMUNICATION

View Article Online
View Journal | View Issue

Check for updates

Cite this: *Mater. Horiz.*, 2020, 7, 928

Received 17th October 2019,
Accepted 2nd December 2019

DOI: 10.1039/c9mh01654f

rsc.li/materials-horizons

A versatile biomaterial ink platform for the melt electrowriting of chemically-crosslinked hydrogels†

Daniel Nahm,[ab] Franziska Weigl,[b] Natascha Schaefer,[c] Ana Sancho,[b] Andreas Frank,[d] Jürgen Groll,[b] Carmen Villmann,[c] Hans-Werner Schmidt,[d] Paul D. Dalton *[b] and Robert Luxenhofer *[ae]

In this study, we designed a novel biomaterial ink platform based on hydrophilic poly(2-ethyl-2-oxazine) (PEtOzi) specifically for melt electrowriting (MEW). This material crosslinks spontaneously after processing *via* dynamic Diels–Alder click chemistry. These direct-written microperiodic structures rapidly swell in water to yield thermoreversible hydrogels. These hydrogels are robust enough for repeated aspiration and ejection through a cannula without structural damage, despite their high water content of 84%. Moreover, the scaffolds retain functional groups for modification using click chemistry and therefore can be readily functionalized as demonstrated using fluorophores and peptides to facilitate visualization and cell attachment. The PEtOzi hydrogel developed here is compatible with confocal imaging and staining protocols for cells. In summary, an advanced material platform based on PEtOzi is reported that is compatible with MEW and results in functionalizable chemically crosslinked microperiodic hydrogels.

New concepts

This research describes how a significant manufacturing limitation for a 3D printing technology is turned into a strength, allowing access to an important class of materials (hydrogels) that has never been reported before for melt electrowriting. The constant elevated heat for melt electrowriting normally has a degradative effect on many important biomedical polymers due to the low flow rates – typically 10–20 μL h^{-1} – required for this processing technology. The presented conceptual shift uses a dynamic process where the hydrophilic polymer material is liquid at high temperature but during the cooling of the molten electrified jet spontaneously crosslinks when printed. We show that the resulting crosslinked hydrogel is non-toxic, can be used to couple *e.g.* peptide sequences, fluorophores and potentially many interesting biomolecules. This hydrophilic, chemically crosslinked hydrogel combines softness desirable for soft tissue engineering with a pronounced structural resilience, to provide an important class of material for both melt electrowriting and biomedical science. This is also the first study reporting the processing of poly(2-oxazine)s using any manufacturing technology, and this dynamic crosslinking also has utility for other, more common, 3D printing technologies.

Chemically crosslinked hydrogels have revolutionized biomaterials research over the past decades due to their ability to mimic important characteristics of biological environments.[1,2] It has also become apparent that a hierarchical structure is important for the emerging field of biofabrication[3] which extensively uses the bioprinting of hydrogels. Crosslinked hydrogels can be designed able to withstand repeated deformations,[4,5] essential for soft robotics,[6] 4D printing[7,8] and mechanical metamaterials.[9]

Melt electrowriting (MEW) is an additive manufacturing technique that enables (low) micron-scale features with complex hierarchical structures.[10,11] MEW has various advantages and disadvantages compared to other manufacturing technologies[12,13] but can generally be considered a hybrid of melt-extrusion and solution electrospinning.[14] However, to date almost all polymers processed *via* MEW are linear, hydrophobic and non-crosslinked polymers[15–17] with the most common being poly(ε-caprolactone) (PCL).[11,18] While post-processing of hydrophobic MEW scaffolds using UV-crosslinking has been reported,[19] here we describe a functional hydrophilic polymer system, based on poly(2-ethyl-2-oxazine) (PEtOzi), that spontaneously, *i.e.* without any external stimulus, chemically crosslinks at ambient conditions. The direct-written structures are both soft and robust after swelling in water. This represents a self-crosslinking polymer processed *via* MEW

[a] *Functional Polymer Materials, Chair for Advanced Materials Synthesis, Department of Chemistry and Pharmacy and Bavarian Polymer Institute, University of Würzburg, Röntgenring 11, 97070, Germany. E-mail: robert.luxenhofer@uni-wuerzburg.de*
[b] *Department of Functional Materials in Medicine and Dentistry, and Bavarian Polymer Institute, University of Würzburg, Pleicherwall 2, 97070, Würzburg, Germany. E-mail: paul.dalton@fmz.uni-wuerzburg.de*
[c] *Institute for Clinical Neurobiology, University of Würzburg, Versbacherstr. 5, 97078 Würzburg, Germany*
[d] *Macromolecular Chemistry I and Bavarian Polymer Institute, University of Bayreuth, Universitätsstraße 30, 95440, Bayreuth, Germany*
[e] *Soft Matter Chemistry, Department of Chemistry, Helsinki University, 00014 Helsinki, Finland*

† Electronic supplementary information (ESI) available. See DOI: 10.1039/c9mh01654f

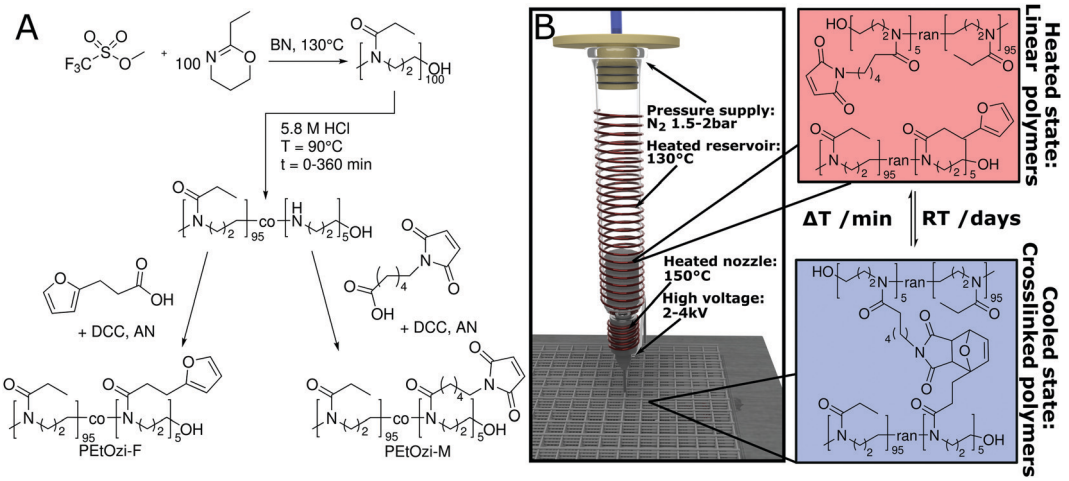

Fig. 1 (A) Synthesis of the furan and maleimide functionalized poly(2-ethyl-2-oxazine) (PEtOzi-M, PEtOzi-F) used in this study (DCC: dicyclohexyl carbodiimide, AN: acetonitrile, BN: benzonitrile). (B) Schematic illustration of the MEW setup, processing conditions and the reversible DA equilibrium allowing liquefaction and melt processing at elevated temperatures followed by the chemically crosslinking upon cooling.

that offers fundamentally different material properties than those previously described.[20]

The spontaneous crosslinking after MEW processing is based on the thermally reversible Diels–Alder (DA) click chemistry of furan and maleimide moieties (Fig. 1A and B).[21,22] The [4+2] cycloaddition of the DA reaction is characterized by an equilibrium between the dienophile and diene, and their bicyclic adduct. This equilibrium depends heavily on external parameters, including temperature[23] and has previously been used for hydrogel formation.[24] For MEW, we identified PEtOzi as a suitable hydrophilic polymer due to its lower glass transition temperature compared to the more commonly used poly-(2-ethyl-2-oxazoline) (PEtOx).[25] This allows a lower MEW processing temperature to reduce thermally induced side reaction during printing. The two prepolymers are synthesized *via* a simple two-step polymer analogue modification similar to the strategy used by Chujo *et al.* (Fig. 1A).[26] Briefly, the living cationic ring-opening polymerization of PEtOzi homopolymers[27,28] is followed by the partial hydrolysis under acidic conditions to result in random poly(2-ethyl-2-oxazine-*co*-propylene imine) copolymers. Subsequently, furan and maleimide moieties, were coupled quantitatively to the secondary amines yielding the biomaterial ink (for detailed characterization, see ESI,† Fig. S1–S4).

After leaving the nozzle, the jet rapidly cools to room temperature, whereby the scaffold gains immediate shape persistence and the equilibrium shifts to the side of the bicyclic adduct resulting in chemical crosslinking (Fig. 1B) necessary for the formation of a hydrogel.

To verify reversible crosslinking, the stretching band of the maleimide double bond (695 cm^{-1}) was observed *via* IR-spectroscopy of a cast film (Fig. 2A). The equilibrium was readily shifted three times without a notable change in the absolute maleimide peak intensity, indicating efficient, reversible crosslinking. Within the limits of detection, no free maleimide could be observed after 2.5 h at 60 °C as the peak intensity decreased essentially to baseline levels. Importantly, the excellent thermal stability of poly(2-oxazine)s (POzi) is particularly favourable for melt processing (Fig. S5, ESI†). The thermal reversibility of the crosslinking could also be followed by differential scanning calorimetry (DSC) (Fig. 2B). The heating trace revealed two broad endothermic peaks between 100 °C and 160 °C which were attributed to the ring-opening of the *endo*- and *exo*-conformation of the bicyclic DA adduct.[29] Due to the low degree of functionalization, these signals were not well resolved. Only after excessive repetitions, non-reversible effects can be observed from DSC. Between the second and third heating cycle

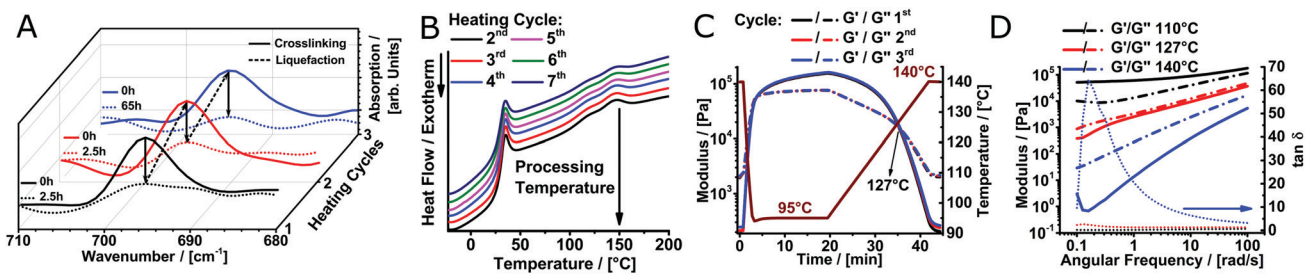

Fig. 2 (A) Monitoring the reversible crosslinking by IR-spectroscopy in three consecutive liquefaction cycles. (B) DSC thermograms of Diels Alder crosslinked poly(2-ethyl-2-oxazine) of seven heating cycles. (C) Temperature-dependant viscoelastic properties of the dynamically crosslinked biomaterial ink investigated by rheology measurements. (D) Frequency dependency of the elastic and viscous moduli at temperatures below, near and above the gel point.

(up to 200 °C), the enthalpy decreased only by 7% from 4.3 J g^{-1} to 4.0 J g^{-1}. However, after seven heating cycles, it decreased to 2.6 J g^{-1}. From a rheological standpoint, however, full thermal reversibility was observed over three consecutive temperature sweeps performed under oxygen and moisture free conditions (Fig. 2C; see ESI† for a detailed discussion). Solidification occurred rapidly upon cooling to 95 °C, while the liquefaction point was found consistently at 127 °C. Temperature-dependent frequency sweeps revealed that at a lower temperature (110 °C), the material showed the typical behaviour of a solid, crosslinked polymer demonstrating a plateau of G' for low frequencies (Fig. 2D). Increasing the temperature to 140 °C drastically decreased the G' at low frequencies, and G' and G'' invert. At this temperature, the material showed the characteristics of a predominantly viscous fluid, corroborating the dynamic nature of the DA crosslinking. It is important to stress that the thermal reversibility of the DA reaction is essential for the application potential of the presented biomaterial ink. However, at elevated temperatures, irreversible side reactions within the polymer melt may occur, which make it difficult to continuously print over an extended time period (see ESI† for a detailed discussion). Thermal degradation or crosslinking is, however, a common challenge for thermal processing, including MEW.[15,19]

Using MEW, microperiodic fibre structures with defined fibre diameter, spacing and number of layers could be obtained. For example, scaffolds with 10 layers and a fibre spacing of 500 μm were direct-written (Fig. 3A). Manufacturing of a scaffold with these dimensions is possible within 7 minutes of printing time. With minor errors in fibre stacking, the structure was highly organized and well-defined. After printing, the scaffolds are insoluble within one hour and were left overnight at room temperature to ensure DA crosslinking. When hydrated with deionized water, swelling was rapid and completed in less than one minute (Video V1, ESI†), with the total scaffold area increasing considerably from 4 cm^2 to 9 cm^2. For better visualization, DY-647P1-Maleimide-coupling gave a blue hue to the scaffold. Notably, the architecture remained undistorted and no fibre delamination was observed (Fig. 3B). This can be attributed to chemical crosslinking between fibres at their junctions, established during fibre deposition, utilizing the dynamic DA reaction. This covalent fibre fusion is an intrinsic feature of the material and greatly improves interlayer adhesion in the printed constructs, which is commonly the mechanically weakest point in a 3D-printed construct.[30,31]

The box-shaped pores increase in size from 500 ± 20 μm to 690 ± 40 μm upon hydration (Fig. 3C and D). We also tested

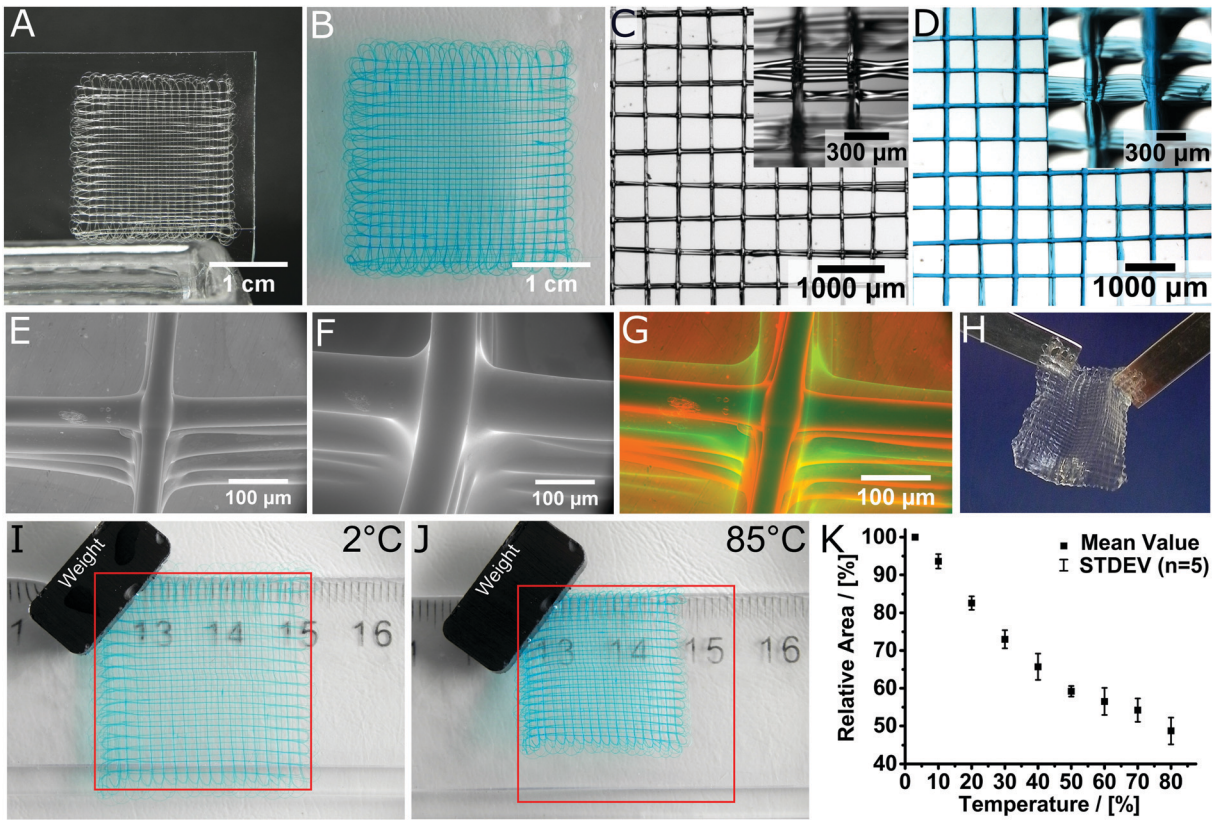

Fig. 3 Layered structure of the MEW printed scaffold in the (A) dry state and (B) swollen state. Stereomicroscopic image of (C) the dry and (D) swollen scaffold, hydrated and stained with DY-647P1-maleimide for improved visualization. Insets show the scaffolds from a tilted angle to better visualize the fibre morphology and stacking. ESEM image of (E) the dried and (F) swollen structure. (G) Visualization of the volume decrease by superposition of the dried and swollen 3D hydrogel scaffold. (H) Scaffolds are mechanically robust and can be easily handled and transferred. Temperature dependent swelling of the hydrogel architectures visualized at (I) 2 °C and (J) 85 °C. The red square indicates the size of the scaffold at 2 °C. (K) Relative area of the scaffolds depending on the temperature. Video 1 (ESI†) shows the hydration process while Video 2 (ESI†) shows the thermoresponsiveness of the samples shown in (I and J).

long-term stability of the scaffolds in deionized water as well as phosphate-buffered saline (PBS) solution and found the samples unaffected after four months of incubation (Fig. S6, ESI†).

Environmental scanning electron microscopy (ESEM) images allow a detailed view on the prepared structures in both, wet and dry state (Fig. 3E–G). In both conditions, the surface morphology of the fibres was smooth and uniform. ESEM also revealed that, accompanied with the increase of the whole scaffold area, the fibres also showed significant increase in mean fibre diameter from 45 ± 5 μm to 89 ± 12 μm after swelling, corresponding to a 290% increase in volume. Using this value, one can estimate an equilibrium water content (EWC) of 74% from ESEM, which compares reasonably well to the EWC of 84 ± 1% determined gravimetrically for the bulk material. Furthermore, the microperiodic hydrogels were durable and could be readily handled (Fig. 3H). When dried at ambient conditions the scaffolds contracted to their original size and remain as light and elastic material (Fig. S7, ESI†).

Due to the inherent thermoresponsive properties of PEtOzi[32] the scaffolds are also stimulus-responsive. The scaffolds area shrinks from about 9 cm^2 to only 4.8 cm^2 (53%) when increasing the temperature beyond physiological temperature (Fig. 3I and J). Swelling and de-swelling occurs within seconds (Video V2, ESI†) and is fully reversible. De-swelling proceeds continuously from 3 °C to 50 °C with a reduction of 10% relative area per 10 °C (Fig. 3K). Beyond 50 °C, de-swelling slows down considerably. This compares well with a reported cloud point temperature for linear PEtOzi of 56 °C.[32] Considering the tunability of the lower critical solution temperature of poly(2-oxazoline) (POx)[33,34] and POzi the de-swelling profile could be tailored for future applications. However, this will likely also require major adjustments in the MEW processing conditions.

It is well-established that cells respond strongly to mechanical cues of their micro environment.[35] Therefore, we evaluated the stiffness of our printed hydrogel fibres by colloidal indentation using an atomic force microscope with the FluidFM® adapted technology as reported elsewhere.[36] Two-layered scaffolds were printed and force-distance curves were measured at >25 random spots on every sample. By fitting a Hertz Model to the force curves, a Young's modulus between 0.140 ± 0.042 MPa and 0.20 ± 0.10 MPa was calculated (Fig. 4A and Fig. S8, ESI†). This value is in line with similar water content hydrogels[37] and contrasts with PCL, which is the most commonly used polymer for MEW to date and has a Young's modulus of 340–365 MPa.[38]

Although these scaffolds are soft hydrogels, they are remarkably robust due to the chemical crosslinking and fibre fusion at the junctions. For example, two-layer scaffolds (Fig. 4B) could be aspirated several times into a syringe *via* a metal needle (14 G). A glass pipette gives visualization as aspirated scaffolds is injected into an aqueous medium without visible structural damage (Fig. 4B–E and Video V3, ESI†). Such properties are highly desirable for an injectable, micro-structured hydrogel implant for ophthalmic and cardiac applications.[39,40] Most importantly, due to the dynamic equilibrium[41] and inevitable imperfect crosslinking of the DA reaction, free furan and maleimide moieties are available for post-processing modification. This gives the opportunity for straightforward modification of the material with fluorescent dyes or biological cues, functionalized with DA functions, maleimide or furan, or thiols utilizing the

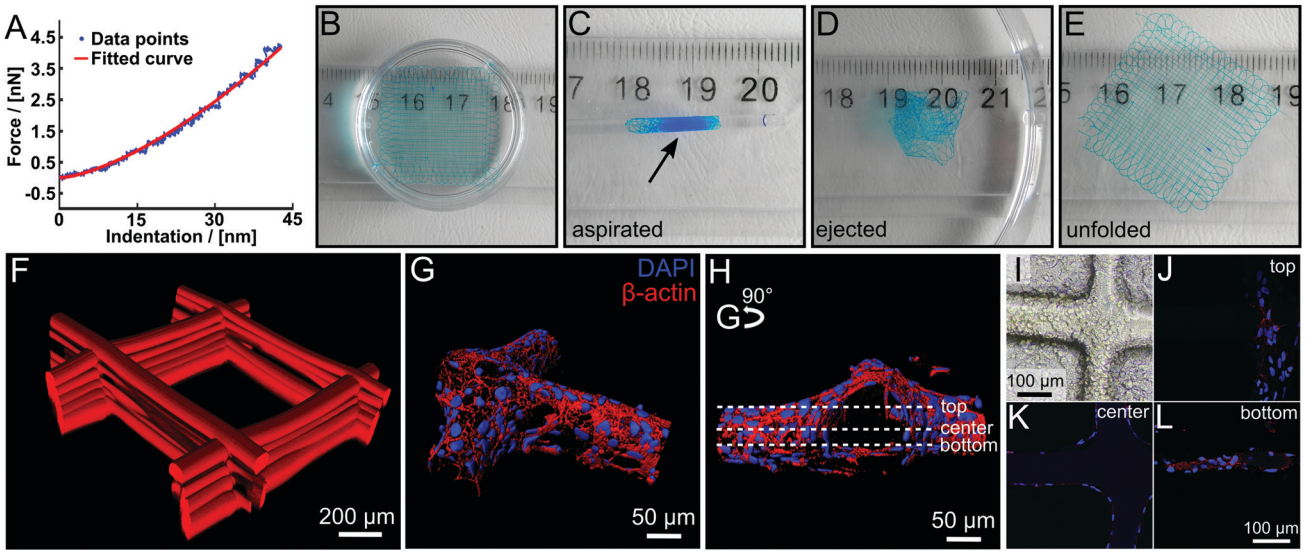

Fig. 4 (A) Example of a force–distance curve for a swollen scaffold with a fitting curve using the Hertz Model. (B–E) Illustration of the robust character of the hydrogel scaffolds. The swollen scaffolds (B) can be aspirated in a glass pipette (inner diameter 1.35 mm) (C) and ejected again repeatedly (D) without any visual damage to the scaffold, which unfolds (E) again by itself. Scaffolds were functionalized with DY-647P1-maleimide for better visualization. (F) Confocal microscope image of a fluorescently labelled hydrogel scaffold with 500 μm fibre spacing. (G–L) HEK293 cells were grown on hydrogel scaffolds functionalized with peptide (NH_2-CGGGRGDS-COOH). (G and H) Cells were stained with cytoskeletal marker protein β-actin (red) and DAPI (nucleus, blue). 3D surface-reconstruction of HEK293 cells attached to scaffold (Imaris 7.6 software). (I) Phase-contrast image of seeded scaffold with HEK293 cells are attached along and around the scaffolds. (J–L) Representative images of one hydrogel filament within the whole scaffold from bottom, center and top are shown, positions marked in (H). Video 3 (ESI†) provides a demonstration of aspiration and ejection, while Video 4 (ESI†) shows (G and H) in greater detail.

Michael addition reaction. The dry scaffolds were simply swollen in an aqueous solution of a maleimide functionalized dye (DY-647P1-maleimide) and incubated overnight. After washing, we were able to visualize the fibres immersed in water, a good solvent for the dye, without leakage. Accordingly modified scaffolds could be visualized *via* confocal microscopy (Fig. 4F).

For the envisioned biomedical applications, biological compatibility is necessary. While obviously the present approach and materials cannot be used to incorporate cells during printing, cells can be added post-processing. It has been established previously that PEtOzi has low cytotoxicity with IC_{50} values between 10 and 100 g L^{-1}.[42] Also, DA based hydrogels have been reported to show low cytotoxicity.[43] Here, the PEtOzi biomaterial ink was evaluated in bulk using a WST-1 elution essay with L929 mouse fibroblasts (see ESI†). Following DIN-ISO 10993-5, cell viability after 48 h of incubation was $\geq 86 \pm 3\%$ (Fig. S9, ESI†), suggesting safety for biomedical applications.

Transfected HEK293 cells are widely used in neurobiological research as a suitable system to investigate the expression and function of proteins. Here, we used this cell line to investigate the growth of HEK293 cells on PEtOzi hydrogel scaffolds. Already four hours after seeding, the attachment to the RGD-functionalized fibres was clearly visible (Fig. 4I). Following four days of growth at the scaffold, HEK293 cells were stained for the cytoskeleton protein β-actin. Nuclear (blue) labelling and β-actin staining (red) allowed 3D re-construction of the cells attached to the scaffold (Fig. 4G, H and J–L and Video V4, ESI†). These experiments highlight that the MEW PEtOzi hydrogel scaffolds are compatible with both, standard cell culture experiments and staining procedures (Fig. 4G and H) while the low cytotoxicity of the polymeric biomaterial ink is corroborated. Furthermore, such smaller fibre diameters are generally more amenable to cell adhesion and proliferation compared to flat substrates or scaffolds made with larger diameters.[44,45]

Considering these results, the MEW-processed PEtOzi scaffolds warrant further research in application-specific scenarios.[46,47] The PEtOzi platform has the potential for tailoring of the material stiffness by altering the swelling degree of the material. This can be realised either by influencing the crosslinking density through the degree of hydrolysis and modification or by adjusting the hydrophilicity of the material. It is important to note that this can be accomplished without changing the basic concept and chemistry presented here. POx and POzi offer the potential for copolymerisation of a large variety of monomers with different side chains, allowing for straightforward tailoring of the hydrophilicity.[48]

In general, MEW allows control over scaffold parameters while maintaining highly aligned fibres and high scaffold porosity.[11,18,45] Our novel approach, to combine MEW with reversible chemical crosslinking offers many new avenues to adjust materials properties without the need for potentially toxic additives such as photoinitiators[49] and allows for straightforward post-processing modification with a readily available maleimide- or furan-modified (bio)(macro)molecules. Other DA-crosslinked hydrogels have also been shown to be biodegradable, the rate of which could tuned by crosslinking density and pH.[41,50] Important to note, the presented PEtOzi system will also have applicability in other additive manufacturing technologies such as fused filament fabrication, where DA crosslinking have demonstrated utility.[31]

Conclusions

In summary, a PEtOzi-based hydrogel platform for the fabrication of soft yet robust 3D microperiodic architectures was established. We consolidated Diels–Alder-click-crosslinking with MEW processing to manufacture chemically crosslinked hydrogels – a new class of material accessible for this additive manufacturing technology. The presented strategy allows straightforward modification post processing, offering the possibility to covalently bind fluorescent markers, catalysts, biological cues or other entities of interest. The fabricated structures have a high equilibrium water content and are surprisingly resilient and readily modifiable. This work lays the foundation for a plethora of different applications in biomedicine and other fields.

Conflicts of interest

The authors have no conflicts to declare.

Acknowledgements

This work was funded by the German Research Foundation (DFG) - Project number 310771104 (awarded to PD and RL). The authors appreciate technical assistance from Christian May, Simone Werner and Dr. Gernot Hochleitner.

References

1 O. Wichterle and D. Lim, *Nature*, 1960, **185**, 117–118.
2 A. S. Hoffman, *Adv. Drug Delivery Rev.*, 2002, **54**, 3–12.
3 J. C. Rose and L. De Laporte, *Adv. Healthcare Mater.*, 2018, **7**, 1701067.
4 J. N. Hanson Shepherd, S. T. Parker, R. F. Shepherd, M. U. Gillette, J. A. Lewis and R. G. Nuzzo, *Adv. Funct. Mater.*, 2011, **21**, 47–54.
5 M. Montgomery, S. Ahadian, L. Davenport Huyer, M. Lo Rito, R. Civitarese, R. D. Vanderlaan, J. Wu, L. A. Reis, A. Momen, S. Akbari, A. Pahnke, R.-K. Li, C. A. Caldarone and M. Radisic, *Nat. Mater.*, 2017, **16**, 1038–1046.
6 C. Majidi, *Adv. Mater. Technol.*, 2019, **4**, 1800477.
7 X. Kuang, D. J. Roach, J. Wu, C. M. Hamel, Z. Ding, T. Wang, M. L. Dunn and H. J. Qi, *Adv. Funct. Mater.*, 2019, **29**, 1805290.
8 A. Kirillova, R. Maxson, G. Stoychev, C. T. Gomillion and L. Ionov, *Adv. Mater.*, 2017, **29**, 1703443.
9 Y. Jiang and Q. Wang, *Sci. Rep.*, 2016, **6**, 34147.
10 P. D. Dalton, *Curr. Opin. Biomed. Eng.*, 2017, **2**, 49–57.

11 A. Hrynevich, B. Ş. Elçi, J. N. Haigh, R. McMaster, A. Youssef, C. Blum, T. Blunk, G. Hochleitner, J. Groll and P. D. Dalton, *Small*, 2018, **14**, 1800232.
12 L. Moroni, T. Boland, J. A. Burdick, C. De Maria, B. Derby, G. Forgacs, J. Groll, Q. Li, J. Malda, V. A. Mironov, C. Mota, M. Nakamura, W. Shu, S. Takeuchi, T. B. F. Woodfield, T. Xu, J. J. Yoo and G. Vozzi, *Trends Biotechnol.*, 2018, **36**, 384–402.
13 T. D. Brown, P. D. Dalton and D. W. Hutmacher, *Prog. Polym. Sci.*, 2016, **56**, 116–166.
14 F. M. Wunner, S. Eggert, J. Maartens, O. Bas, P. D. Dalton, E. M. De-Juan-Pardo and D. W. Hutmacher, *3D Print Addit. Manuf.*, 2019, **6**, 82–90.
15 G. Hochleitner, J. F. Hümmer, R. Luxenhofer and J. Groll, *Polymer*, 2014, **55**, 5017–5023.
16 J. N. Haigh, T. R. Dargaville and P. D. Dalton, *Mater. Sci. Eng., C*, 2017, **77**, 883–887.
17 S. Florczak, T. Lorson, T. Zheng, M. Mrlik, D. W. Hutmacher, M. J. Higgins, R. Luxenhofer and P. D. Dalton, *Polym. Int.*, 2019, **68**, 735–745.
18 T. D. Brown, P. D. Dalton and D. W. Hutmacher, *Adv. Mater.*, 2011, **23**, 5651–5657.
19 F. Chen, G. Hochleitner, T. Woodfield, J. Groll, P. D. Dalton and B. G. Amsden, *Biomacromolecules*, 2016, **17**, 208–214.
20 T. M. Robinson, D. W. Hutmacher and P. D. Dalton, *Adv. Funct. Mater.*, 2019, **29**, 1904664.
21 A. Gandini, A. Silvestre and D. Coelho, *Polym. Chem.*, 2013, **4**, 1364–1371.
22 H. C. Kolb, M. G. Finn and K. B. Sharpless, *Angew. Chem., Int. Ed.*, 2001, **40**, 2004–2021.
23 V. Froidevaux, M. Borne, E. Laborbe, R. Auvergne, A. Gandini and B. Boutevin, *RSC Adv.*, 2015, **5**, 37742–37754.
24 L. J. Smith, S. M. Taimoory, R. Y. Tam, A. E. G. Baker, N. Binth Mohammad, J. F. Trant and M. S. Shoichet, *Biomacromolecules*, 2018, **19**, 926–935.
25 M. M. Bloksma, U. S. Schubert and R. Hoogenboom, *Macromol. Rapid Commun.*, 2011, **32**, 1419–1441.
26 Y. Chujo, K. Sada and T. Saegusa, *Macromolecules*, 1990, **23**, 2636–2641.
27 B. J. Adzima, H. A. Aguirre, C. J. Kloxin, T. F. Scott and C. N. Bowman, *Macromolecules*, 2008, **41**, 9112–9117.
28 A. Aguado, J. Boulos, A. Carreras, A. Montoya and J. Rodriquez, *J. Heterocycl. Chem.*, 2007, **44**, 1517–1520.
29 K. Sugane, N. Kumai, Y. Yoshioka, A. Shibita and M. Shibata, *Polymer*, 2017, **124**, 20–29.
30 G. A. Appuhamillage, J. C. Reagan, S. Khorsandi, J. R. Davidson, W. Voit and R. A. Smaldone, *Polym. Chem.*, 2017, **8**, 2087–2092.
31 K. Yang, J. C. Grant, P. Lamey, A. Joshi-Imre, B. R. Lund, R. A. Smaldone and W. Voit, *Adv. Funct. Mater.*, 2017, **27**, 1700318.
32 M. M. Bloksma, R. M. Paulus, H. P. C. van Kuringen, F. van der Woerdt, H. M. L. Lambermont Thijs, U. S. Schubert and R. Hoogenboom, *Macromol. Rapid Commun.*, 2012, **33**, 92–96.
33 J.-S. Park and K. Kataoka, *Macromolecules*, 2007, **40**, 3599–3609.
34 S. Huber and R. Jordan, *Colloid Polym. Sci.*, 2008, **286**, 395–402.
35 K. Franze, *Development*, 2013, **140**, 3069–3077.
36 A. Sancho, I. Vandersmissen, S. Craps, L. Aernout and J. Groll, *Sci. Rep.*, 2017, **7**, 46152.
37 C. Cha, S. Y. Kim, L. Cao and H. Kong, *Biomaterials*, 2010, **31**, 4864–4871.
38 S. Eshraghi and S. Das, *Acta Biomater.*, 2010, **6**, 2467–2476.
39 M. K. Yoo, Y. J. Choi, J. H. Lee, W. R. Wee and C. S. Cho, *J. Drug Delivery Sci. Technol.*, 2007, **17**, 81–85.
40 M. J. Seiler and R. B. Aramant, *Prog. Retinal Eye Res.*, 2012, **31**, 661–687.
41 S. Kirchhof, F. P. Brandl, N. Hammer and A. M. Goepferich, *J. Mater. Chem. B*, 2013, **1**, 4855–4864.
42 Z. Kroneková, T. Lorson, J. Kronek and R. Luxenhofer, *ChemRxiv*, 2018, DOI: 10.26434/chemrxiv.5793990.v1.
43 C. M. Nimmo, S. C. Owen and M. S. Shoichet, *Biomacromolecules*, 2011, **12**, 824–830.
44 T. L. Jenkins and D. Little, *npj Regener. Med.*, 2019, **4**, 15.
45 G. Hochleitner, T. Jüngst, T. D. Brown, K. Hahn, C. Moseke, F. Jakob, P. D. Dalton and J. Groll, *Biofabrication*, 2015, **7**, 035002.
46 O. Bas, I. Catelas, E. M. D. Juan-Pardo and D. W. Hutmacher, *Adv. Drug Delivery Rev.*, 2018, **132**, 214–234.
47 E. Spedden and C. Staii, *Int. J. Mol. Sci.*, 2013, **14**, 16124–16140.
48 M. Glassner, M. Vergaelen and R. Hoogenboom, *Polym. Int.*, 2017, **67**, 32–45.
49 M. Gregoritza and F. P. Brandl, *Eur. J. Pharm. Biopharm.*, 2015, **97**, 438–453.
50 S. Kirchhof, A. Strasser, H.-J. Wittmann, V. Messmann, N. Hammer, A. M. Goepferich and F. P. Brandl, *J. Mater. Chem. B*, 2015, **3**, 449–457.